Crowd Control of Ions in the Astral Analyzer

Authors: Hamish Stewart*, Dmitry Grinfeld, Johannes Petzoldt, Bernd Hagedorn, Michael Skoblin, Alexander Makarov and Christian Hock. *Thermo Fisher Scientific, Bremen, Germany.*

Abstract

Space charge effects are the Achilles' heel of all high-resolution ion optical devices. In time-of-flight mass analyzers these may manifest as reduction of resolving power, mass measurement shift, peak coalescence and/or transmission losses, whilst highly sensitive modern ion sources and injection devices ensure that such limits are easily exceeded. Space charge effects have been investigated, by experiment and simulation study, for the Astral multi-reflection analyzer, incorporating ion focusing via a pair of converging ion mirrors, and fed by a pulsed extraction ion trap. Major factors were identified as the resonant effect between ~10^3 ions of similar m/z in-flight, and the expansion of trapped packets of ~10^{4-5} ions prior to extraction. Optimum operation and compensated ion mirror calibration strategies were then generated and described based on these findings.

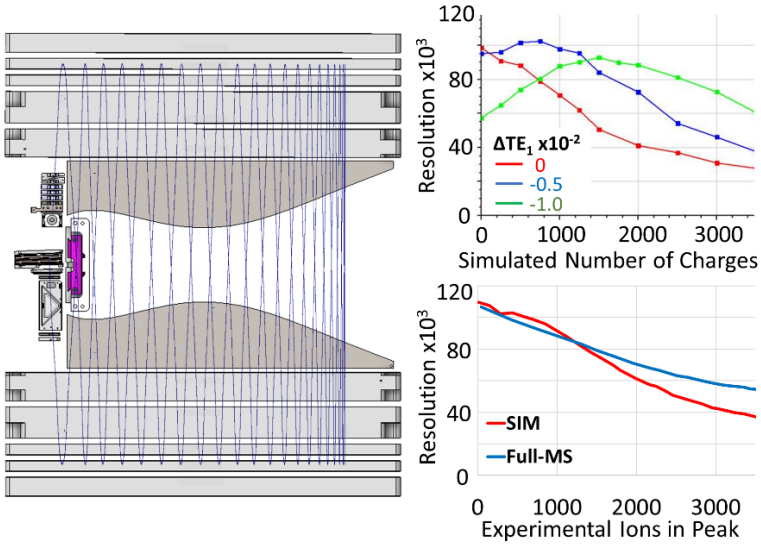

Introduction

Complex biological mixtures typically present a challenging concentration range of analyte materials to any mass spectrometer, for example human plasma protein abundance covers at least ten orders of magnitude dynamic range[1]. Whilst sample preparation strategies such as fractionation may reduce this burden[2], and the number of ions delivered to the mass analyzer attenuated via automatic gain control processes[3], it remains necessary to tolerate a range of ion intensities. This is especially so for high throughput studies, such as modern bottom-up proteomics[4], that deliver large amounts of chromatographically separated sample over very short experimental cycles, compressed down to 5-minute separations.

Space charge effects are a major limiter of mass analyzer dynamic range. In Orbitrap™ analyzers[5,6], a widely used form of electrostatic trap for example, a high overall number of injected ions raises the average potential within the device, reducing the ion oscillation frequency and causing a (largely correctable) ~+1 ppm m/z measurement shift across all peaks per ~10^5 charges. Coupling of oscillation frequencies between ions of like, or merely similar m/z then generates less intuitive resonant effects such as self-bunching and coalescence at ~10^4 charges in-peak[7].

Reflectron time-of-flight (ToF) analyzers[8,9], particularly multi-reflection MR-ToF analyzers which offer long folded flight paths and far higher resolving power[10-13], also suffer from these influences. These analyzers isochronously focus ions of divergent energy to a detector plane via one or multiple reflections from ion mirrors, a process similar to the isochronous oscillation within Orbitraps but extremely intolerant to shift in the position or quality of the focal plane. Instead of relatively benign self-bunching, in-peak resonant space charge causes loss of resolution at ~10^2 charges. This was thought to occur due to loss of the temporal focus as ions of divergent energy are pushed to higher/lower amplitude respectively, causing times-of-flight to shift as a function of energy, degrading and effectively drawing the focal plane away from the detector surface[14]. Coalescence effects in MR-ToF analyzers are also very much in evidence, for example merging the MRFA peptide doublet at m/z 526.26 and 526.27 with less than 10^3 charges in the doublet[15].

ToF analyzers typically incorporate an ion preparation and extraction device that have their own space charge related influences. For example, the common orthogonal extraction process, that pulls segments out of a continuous (or modulated/bunched) ion beam, may inject ions at very high repetition rates with usually high transmission losses[16], and leave little fear of exposing the analyzer to strong space charge effects – though these may still be notable[17]. On the other side, extraction ion traps such as the C-Trap[18] may accumulate ions for a prolonged period, requiring several milliseconds for processing before pulse-extracting the entire ion set directly into the analyzer.

Intuitively, the space-charge effects relate to the density of ions within the analyzer. It follows that a mass analyzer that allows the ion packets to widely disperse should have an inherent advantage in space charge tolerance versus those that keep the ion beam transversally compressed. One such multi-reflection device, the Astral™ analyzer, has been described whereby ions oscillate between a pair of converging elongated ion mirrors whilst drifting down the elongate channel[19]. The ions spread out widely as they drift, but the mirror convergence deflects the drifting ions back with every oscillation, eventually reversing the drift velocity and focusing them to a detector. Fed by an extraction ion trap, performance of this mass analyzer with increasing space charge has been investigated via experiment and simulation, and the influences of both resonant and non-resonant effects analyzed.

Methods

Experiments were performed using a prototype version of the Thermo Scientific™ Orbitrap Astral mass spectrometer[20]. The mass analyzer[19] is a tabletop sized assembly shown in Figure 1a, through which ions follow a zig-zag flight path. Electrosprayed analyte ions were isolated by a quadrupole mass filter, transferred via an ion guide, and accumulated in the ion processor, which incorporates a collision region and a pulsed extraction ion trap. This latter device is a 10 cm long linear quadrupole RF ion trap with a 2mm inscribed radius. The trap structure is shown in Figure 1b. Radial trapping was performed by a 3.7 MHz, 250-1800 $V_{peak\text{-}peak}$ RF waveform. Most notably the RF(-) electrodes are split equatorially, and the opened spaces on either side host a pair of auxiliary DC electrodes, which are wedged to trap ions longitudinally in the central region for following extraction [21-22]. Ions were extracted into the analyzer through an extraction slot by +/-900V pulsed "push and pull" voltages applied to the opposing halves of the trapping structure.

On entering the Astral analyzer system, the beam was accelerated to 4 keV and shaped by a pair of lenses whilst a pair of prism-shaped deflectors set the angle at which the ions oscillated between the two elongate mirrors. The ions drifted down the gap between the mirrors and dispersed under their thermal velocity spread. The convergence of the two mirrors, induced by a 200 µm thick spacer, reduced the drift rate of each ion, and its drift was eventually stopped at a distance L from the point of injection. The drift distance constituted from 310 to 360 mm (with an average of 335 mm) depending on the angle of injection within its intrinsic spread. Noteworthy, the drift expansion of the ion population was not counteracted until the stopping point which resulted in a considerably wide spatial dispersion up to 50 mm, a key point of minimization of the Coulomb repulsion forces in the ion bunch.

During the drift expansion, the size of the ion bunch substantially exceeds the distance between the trajectories on different oscillations as the latter tends to shrink as the drift velocity decreases. Therefore, the ion populations on different oscillations overlap in space. Nevertheless, the optimized convergence of the mirrors and a set of specially shaped electrodes, referred to as Ion Foil, cause the drift spread to reduce on the way back from the drift reversal point, so that the ions arrive at the detector as a single bunch focused both spatially and temporally. The analyzer was tuned so that the ions underwent 24 oscillations between the mirrors resulting in a 30m flight path.

In our experiments the ions were generated from an electrosprayed solution. In some experiments we used the Pierce™ Flexmix™ calibration solution containing caffeine, MRFA peptide and Ultramark polymer. In other measurements, we used Angiotensin dissolved in 50:50 ACN:H_20. Depending on whether the Coulomb interaction between ions or different m/z was in question, the ionic species were isolated in a quadrupole mass filter or not. The numbers of ions to be sent to the analyzer and, correspondingly their total charge, were selected by scanning the accumulation time in the ion trap before ejection. The control of ion numbers was done by measuring the peak intensity and dividing it by a preliminarily calibrated single-ion response.

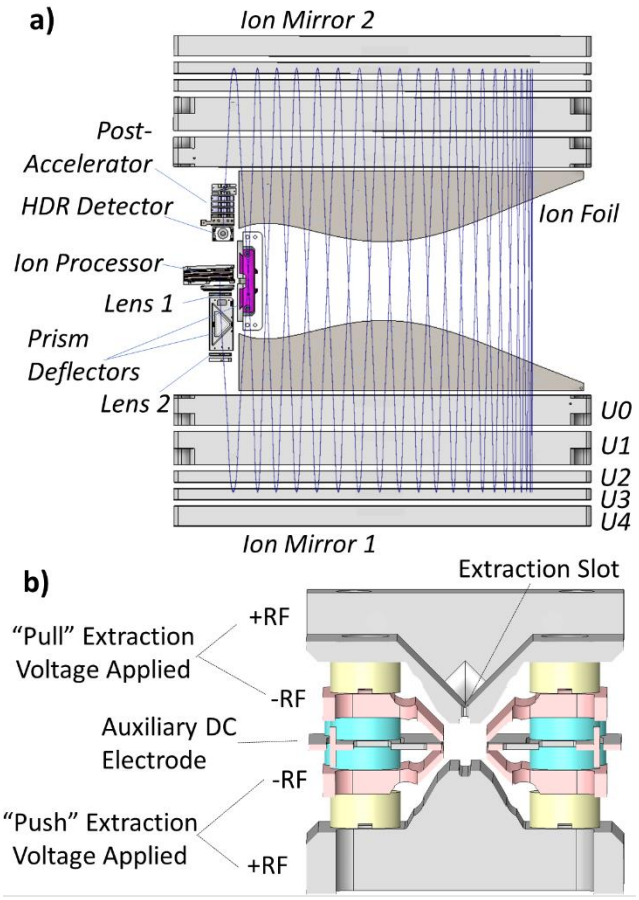

Figure 1. Schematic diagram of the tabletop sized mass analyzer.

Mirror Calibration: Practical optimization of multi-stage ion mirrors provides a challenge of accounting for mechanical deviations, maximizing energy acceptance and aligning the focal plane to the detector surface[23-25]. Each mirror was composed of 5 electrodes, one grounded U_0, one strongly accelerating to provide spatial focusing U_1, and three reflecting $U_{2\text{-}4}$. Mirror potentials were optimized in simulation as a function of ion energy ε_0 producing a coefficient C for each electrode shown in Table 1. The set of coefficients C was optimized to produce a flat dependence of the oscillation time T vs. the ion energy in an interval of $4000\,V \pm 100\,V$. Besides that two correction vectors δC(1) and δC(2) were found. Application of electrode voltages according to Equation 1 modifies the flat energy dependence in a controllable manner. So, the parameter TE_1 shifts the first derivative of the arrival time with respect to ion energy, effectively moving the focal plane position, allowing the resolution sweet spot to be found. TE_2 shifts the second derivative, altering the position of this focal plane with respect to ion energy.

The advantage here is that the analyzer could be broadly calibrated from a general starting point, by modifying the parameters TE_1 and TE_2

$$\begin{bmatrix} U_1 \\ U_2 \\ U_3 \\ U_4 \end{bmatrix} = \varepsilon_0 \left\{ \begin{bmatrix} {C_1}^{(0)} \\ {C_2}^{(0)} \\ {C_3}^{(0)} \\ {C_4}^{(0)} \end{bmatrix} + TE_1 \begin{bmatrix} {\delta C_1}^{(1)} \\ {\delta C_2}^{(1)} \\ {\delta C_3}^{(1)} \\ {\delta C_4}^{(1)} \end{bmatrix} + TE_2 \begin{bmatrix} {\delta C_1}^{(2)} \\ {\delta C_2}^{(2)} \\ {\delta C_3}^{(2)} \\ {\delta C_4}^{(2)} \end{bmatrix} \right\}$$

Equation 1.

	C	$\delta C^{(1)}$	$\delta C^{(2)}$
U_1	-1.840	5.67	-0.256
U_2	-1.158	-1.616	-0.654
U_3	0.916	-0.715	0.032
U_4	1.503	-2.963	-0.361

Table 1. Mirror potentials and perturbation coefficients as function of energy.

Calibration was performed via injection of isolated ions (normally the MRFA peptide), scanning of TE_1 and ion energy to record the loci of best resolution (minimal peak width), that indicates a first-order temporal focusing. These loci form generally a wavy line which is approximately described by a cubic function as shown in Figure 2a-c, whose shape varies under different values of the parameter TE_2. The optimal values of both tuning parameters correspond to zero inclination of the wavy line in the point of inflection as illustrated in Figure 2B. Such regime generates the third-order temporal focus and provides, correspondingly, the best possible resolving power of the analyzer.

Beyond merely achieving a good calibration, the time-energy inclination defined by the parameter TE_1 shifts the focal plane in a controllable way.

As shown in previous study[26], the primary effect of the space-charge load consists in alteration of the focal plane position which may be roughly corrected by adjusting a single potential. The specific parametrization of all four potentials according to Equation 1 provides an accurate way of such adjustment by a proper choice of TE_1 which doesn't affect other focusing properties of ion mirrors.

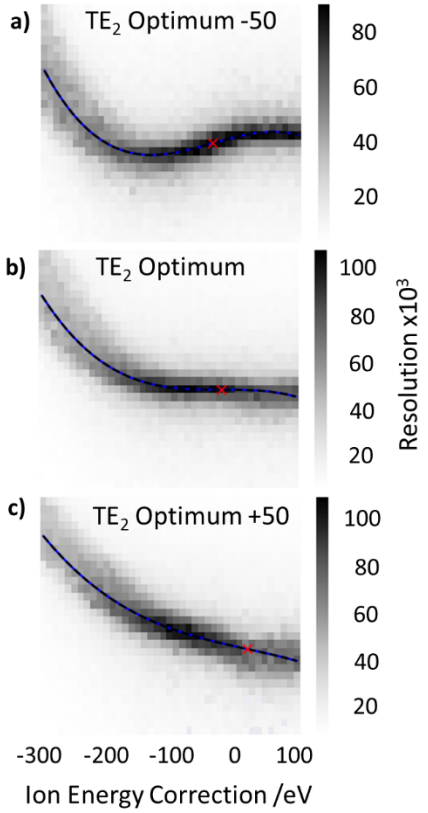

Figure 2. Energy acceptance curves (Trap offset adjustment vs TE_1 resolution plot) for differing TE_2 values.

Simulation: Simulations of space charge effects were constructed using the using the MASIM3D software package, both to model trapped ion spatial distributions within the RF ion trap[27] and resonant influences between ions of like or similar m/z within the mirror system[7,15].

Result and Discussion

Space Charge Effects in the Ion Processor: Figure 3 shows a simulation of axial and radial ion distributions in the extraction trap with a 2mm inscribed radius and the 1000 $V_{p\text{-}p}$ RF waveform applied at 4.5 MHz. The axial trapping was realized with a -5V bias applied to 4 mm-long auxiliary DC electrodes that protrude into the trapping region as shown in Fig. 1. The trapped ionic species were a 1:1:1 mixture of m/z 195, 524 and 1522, which correspond to key analyte species within the Flexmix solution: caffeine, MRFA and ultramark.

At 30k trapped charges, there is very little axial difference in the DC controlled axial distributions, whilst the radial distributions vary greatly due to the m/z dependencies of RF trapping – namely the shallower well depth for higher m/z. As the number of charges increased to 100 and 300k (both beyond the linear capacity of the device[21]), increased Coulomb repulsion acts against the radially constraining RF pseudopotential and the axially constraining DC field. As a result, the ion spreads widen in both radial and axial dimension. The effect is not uniform for all ion types, however; the highest m/z ions (1522 Da) experience the greatest radial expansion due to a weaker RF confinement, which is known to be inversely proportional

to m/z. The Coulomb interaction between different species also makes the higher m/z ion densities assume an 'onion ring' structure with a depleted center as the repulsion from the low m/z ion drives them out of the trap's axis.

This is broadly the expected behaviour, radial stratification by m/z having been previously described for RF ion traps[28]. The axial elongation of the trapped ion cloud is also somewhat mass dependent, in spite of the DC potential, as the charge density varies with the radial trapping RF pseudopotential. The radially compressed low m/z ions are squeezed out of the axial trapping well.

For injection into the Astral analyzer, these space charge effects will push high m/z ions to disproportionately higher energy spreads and increase turnaround time, likely reducing resolution. On the flip side, charge density will also reduce preferentially for the higher m/z ions, which might grant an improved tolerance to resonant space charge influences within the analyzer, after pulsing ions out of the trap.

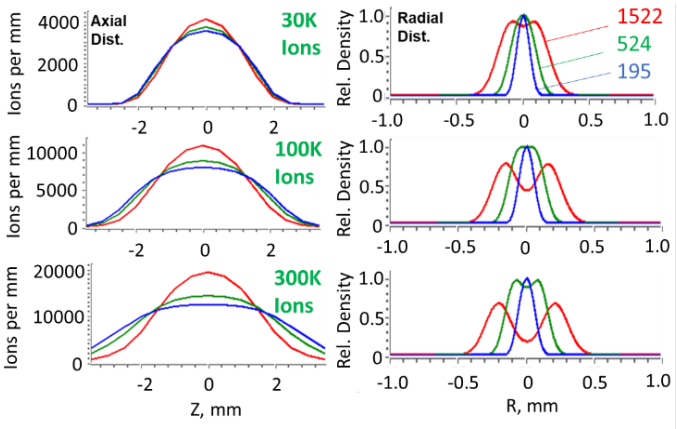

Figure 3. Simulated ion axial and radial distributions for an equal mixture of m/z 195, 524 and 1522 under space charge, within an ion trap with 4mm auxiliary DC trapping electrodes at -5V.

Resolution and Mass Accuracy Trends: For measurement of resonant (single m/z ion packet) effects, isolated MRFA ions were injected into the Astral analyzer with different ion accumulation times, and the resolution and peak shape compared for differing ion quantities. A second experiment to this single ion monitoring (SIM) test was carried out in which the quadrupole isolation window was opened up to admit a full m/z 150-2000 range of FlexMix calibrant ions, to share both trapping and flight stages with the MRFA ions. In simulation, bunches of m/z 524 ions were flown through a simulacrum of the analyzer, albeit with 22 oscillations rather than the usual 24. Varying amounts of charge were given to the particles for the purposes of space charge calculations, and peak resolutions calculated based on time distributions through a detector plane. The mirror focusing parameter TE_1, which shifts the position of the focal plane, was adjusted over two repeat experiments in an attempt to harden the analyzer to space charge. Figure 4a shows the results of the simulations, while 4b shows the experimental results.

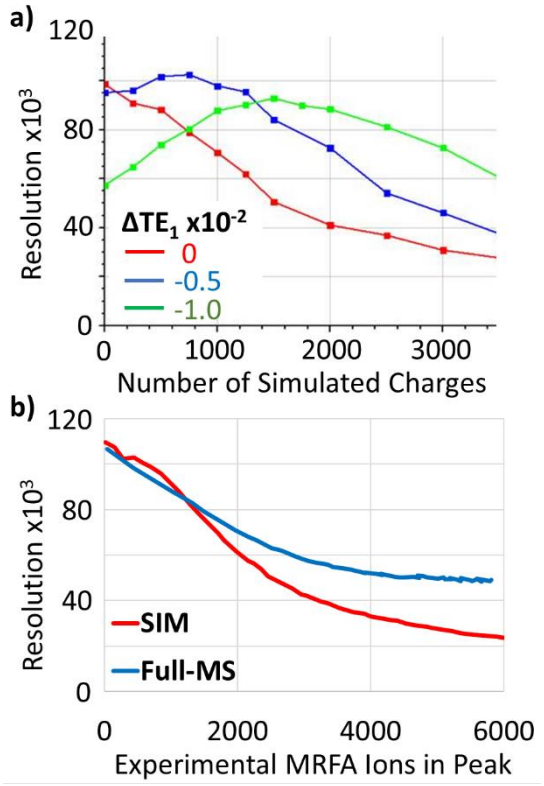

Figure 4. Simulated m/z 524 peak resolution loss with number of charges in peak.

Simulated resolution drops off markedly for a system with no hardening to space charge, halving from 100K to <50K by 1500 charges. A slight shift to TE_1 (-0.005) almost doubles this tolerance range, with little cost to low charge resolving power. A large TE_1 shift (-0.01) both ruins low space charge performance and reduces the maximum peak resolving power but improves high-charge performance.

The experimental trace matches the simulation in performance, though more closely resembles the slightly hardened TE_1-0.005 plot than the zero-space charge optimum. This small shift may simply be due to the space charge inherent in the TE_1 calibration. Remarkably the space charge performance appears to substantially improve for the full-MS experiment. The 50K resolving power crossing point was almost doubled, from 2500 to 5000 ions in peak, when the MRFA trapped ion cloud was broadened by other calibrant ions. An important consideration raised from the simulation results in Figure 3 was that the conditions in the extraction trap, particularly space charge from the distribution of different trapped ions, could influence behaviour in the ToF analyzer. The most straightforward explanation is that broadening of the trapped ion volume under space charge helps mitigate resonant space charge effects in the analyzer, as the initial density of like m/z ions is reduced, and thus charge density of ions in flight is reduced.

The full picture of this enhanced space charge resilience is however likely less rosy, as low ion number packets will also find themselves expanded by competing calibrant ions, and their peaks likely suffer a lower resolution than were they isolated.

Another method to expand the ion cloud is to reduce the RF amplitude, and reduce the depth of the trapping pseudopotential well. Supplemental Figure 1 shows this influence on MRFA space charge behaviour, whereby a deeper well depth reduced space charge resilience and a shallower depth increased it. The effect was surprisingly close to simply modifying TE_1, supporting the hypothesis. There appears a temptation to thus lower RF amplitude and enjoy better space charge behaviour, but in practice a high RF amplitude is generally preferred for trapping efficiency and ion capacity. It may be a worthwhile strategy for isolated ion targeted SIM experiments however, where the total ion number is limited and the ion processor's capacity not heavily utilised.

It is clear that peak resolution drops with space charge, but it is also important to understand the influence on peak shape. Figure 5 shows a series of averaged m/z 524 peaks, taken from ions of the isolated MRFA peptide measured with increasing accumulation time. The detector of the Astral analyzer splits the signal into two channels, which are separately amplified/attenuated to have a 10x difference in gain between them. The blue high gain trace is shown along with the orange low gain trace, which it matches until the point of saturation. In normal operation data from saturated peaks is discarded in favor of the low gain channel.

Initially peaks grow smoothly with little loss of resolution, but above ~500 ions this loss accelerates until eventually slowing down again at several thousand ions. There was little m/z shift observed. Most notably the loss of resolution appeared to manifest in a move in the peak shape from near-gaussian to an almost flat-topped shape. At 10,000 ions in peak there was even the beginnings of peak bifurcation. Previous experiments shown in Supplementary Figure 2, and carried out before the full implementation of the mirror calibration procedure, showed true peak splitting at around 5,000 ions in peak, along with a significant ~5 ppm m/z shift. It is possible that poor matching of the ion energy with the mirror acceptance could produce m/z shifts, though the bifurcation effect is a challenge to explain. Fortunately with well-tuned mirrors it seems not to be strongly in evidence.

Loss of resolution with peak intensity has at least one major benefit, in that it reduces the burden of detector dynamic range. Peak height stopped growing at equivalent 3V in Figure 5, and afterwards merely broadened, which would afford a detector and associated digitizer a considerable serendipitous enhancement of dynamic range. If low m/z suffered more severe resolution loss than high m/z, that would be all the better for the detector, as low m/z ToF peaks are taller and narrower than high m/z counterparts.

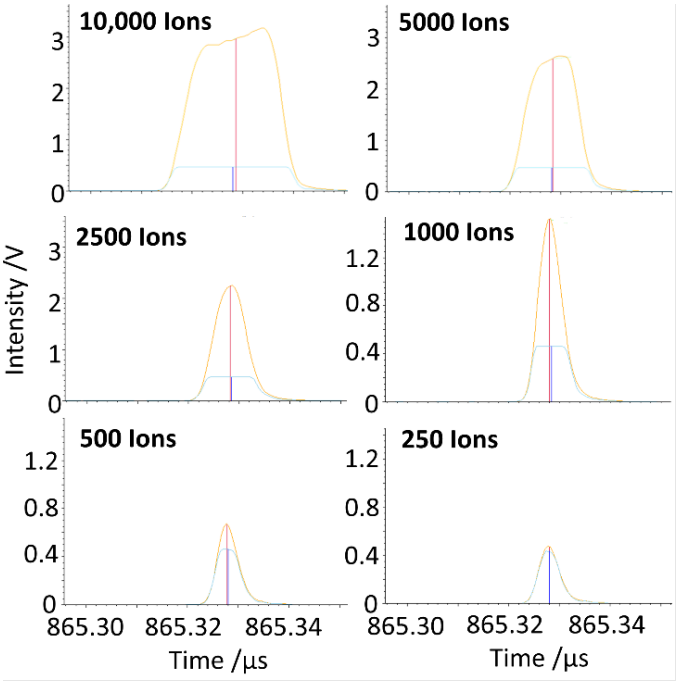

Figure 5. Influence of resonant (in-peak) space charge m/z 524 peak shape.

As a function of overall injected ion number, average resolution has been shown to exceed 80k, and m/z measurement remain stable to the ion processor's linear limit of 50,000 ions[20], as shown in Supplementary Figure 3. At extreme ion loads, where the trap is saturated, not only does resolution of the highly intense peaks continue to fall, but significant mass shifts start to manifest. Figure 6 shows Flexmix mass spectra taken with 10,000 and 100,000 ions detected per shot, with a m/z range of 150-2000 and 1000 V_{p-p} RF. This ion load is easily sufficient to induce space charge broadening. It can be seen that all the peaks remain present, but that low m/z suffers the greatest loss of resolution, as might be predicted from the greater low m/z charge density within the RF trap (as these ions sit in a deeper RF pseudopotential well). Among higher m/z ions, there was a substantial positive m/z shift, likely related to the severe initial ion spatial distribution distortion revealed in Figure 3.

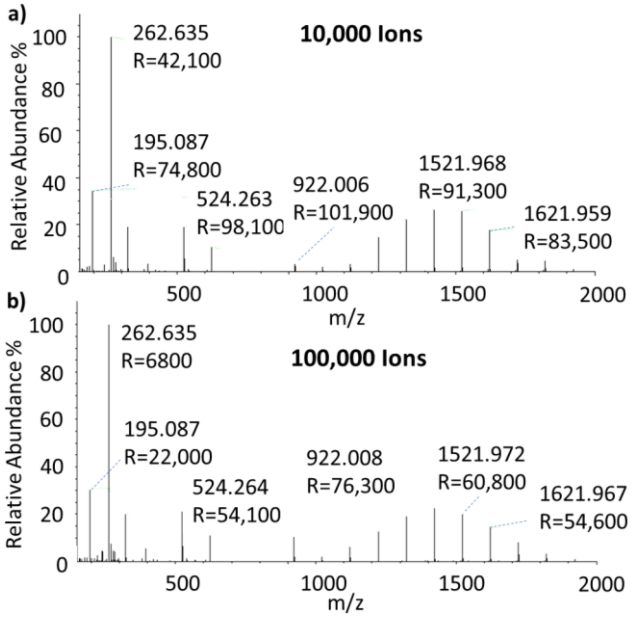

Figure 6. ToF intensity and profile mass spectra of 10,000 and 100,000 detected ions of Flexmix™ calibration solution.

Balanced Mirror Tuning: Figure 7 reports the influence of adjusting the TE_1 parameter from its calibrated optimum of -19.0, on in-peak space charge resilience for a range of FlexMix ions measured in full-MS mode. Again, data were acquired via a single scan of trap accumulation time. The RF amplitude was a relatively low 1000 V, and the total number of detected ions spanned from 5k to 130k. A slight hardening of the mirror, a more negative TE_1, served to help the lower m/z (highest charge density) peak resolution, but hindered higher m/z measurement. Positive TE_1 caused damage across the board. Perhaps surprisingly, the TE_1 value that gave the best low space charge resolution result also gave the best overall high space charge performance.

For mass accuracy, generally this was very good, but at very high ion loads (>50K) the higher m/z ions began to drift upwards. This trend wasn't observed in earlier scans of ion number that used a higher 1400 V RF amplitude, such as that depicted in supplementary Figure 3. Likely this is due to the trap charge capacity being almost 2x higher, with high m/z species less forced out to high radial displacement. For most proteomics studies, with a relatively high (>300) first mass for full MS survey scans, this is unlikely to be an issue as the maximum 1800 V RF amplitude is used. The possibility of such error should however be borne in mind for survey scans with a low first mass / low RF amplitude, and m/z range or ion number set accordingly.

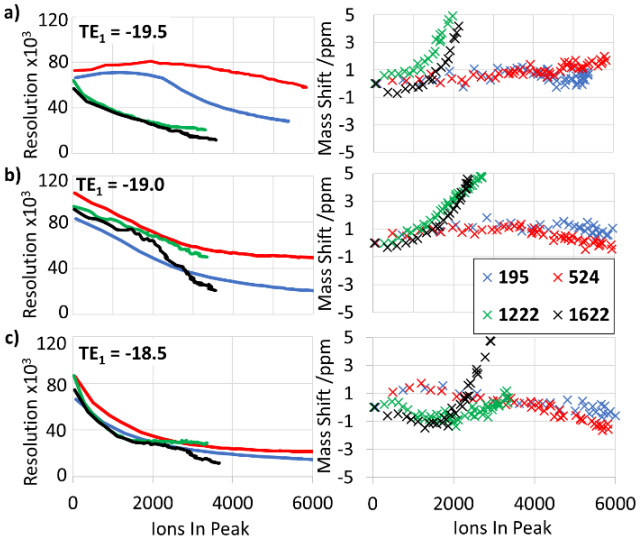

Figure 7. Space charge effects suffered by several different m/z Flexmix ions during Full-MS scans of ion accumulation time, at varying TE1 ($x10^{-2}$) values.

Coalescence: Coalescence is a counter-intuitive phenomenon whereby repulsion between ions oscillating within a potential well brings them closer together, as oscillation frequencies synchronize. In Orbitrap instruments the coalescence threshold is typically measured by looking at the second isotope of the MRFA peptide, m/z 526, which manifests a doublet separated by only 11 mDa, and requiring very high resolution to separate. Figure 8 shows the simulated evolution of coalescence within an approximation of the MRFA isotopic doublet, composed of 1500 particles of m/z 526.26 and 1000 of m/z 526.27, both as ion arrival histograms and in terms of phase diagrams of the ion bunch. At zero charges the ion arrival times (analogous to instantaneous position) are flat with respect to energy, showing good alignment of the time focus with the detector plane. However, by 2008 charges the peak width was markedly broadened, and the arrival times clearly tilted with respect to energy, showing that the focal plane had become shifted and misaligned from the detector plane. At the next step of 2920 charges, the two peaks become strongly overlapping, having largely coalesced by 3330 charges.

The rotation of the ions' time-energy phase space at the detector surface may be rationalised. The ions which have a higher kinetic energy upon injection oscillate with higher amplitudes and penetrate deeper into the electrostatic mirrors. They spend most of the time farther from the analyzer's middle plane and experience a Coulombic force from the other ions directed outwards. As a result, the oscillation period of these ions becomes somewhat longer. Correspondingly, the low-energy ions experience predominantly inwards-oriented Coulomb forces that shorten their oscillation periods. The impact of strengthening the mirror parameter TE_1, which defines the time-energy correlation and has been shown to harden the analyzer to such space charge effects, is that it applies a counter phase space rotation.

In a cluster of peaks, a low abundance peak may be expected to experience this peak broadening in the presence of a nearby abundant peak. Second, the Coulomb repulsion also re-distributes the energy between ions, increasing it for smaller m/z and decreasing for

higher m/z ions in a cluster of close peaks. In Fourier Transform Mass Spectrometry (FT MS), the energy coupling leads to the self-bunching and coalescence effects as oscillation frequencies for different m/z ions come into alignment.

Figure 9 shows experimentally acquired peak shapes for the same doublet. The initial overlap is greater than in the simulation, likely because the real isotopic envelope is much more complex than the simple simulation, with several smaller underlying isotopic species. Peak broadening by 2000 ions pushes the doublet to almost overlap completely, by which point the automatic peak deconvolution ceases to recognize a doublet, and there is a ~1ppm mass shift observed (Supplementary Figure 4). The envelope is completely merged by 3000 ions. The loss of resolving power under space charge is currently a much more significant limitation than coalescence for separating closely spaced species, though improvements to unlock higher resolving power, for example via a multi-pass "zoom" mode[29], may shift this balance.

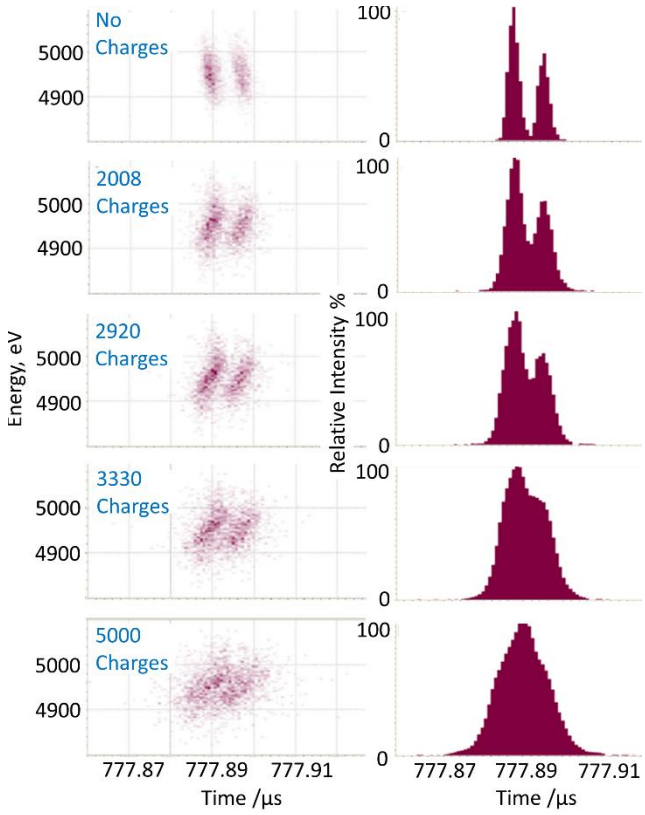

Figure 8. Simulated peak histograms for the MRFA second isotopic doublet, showing resolution loss and eventual coalescence under increasing space charge.

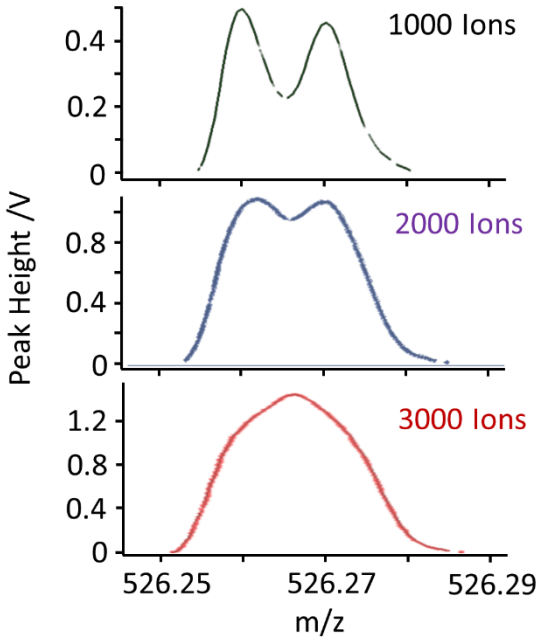

Figure 9. m/z 526 MRFA doublet coalescence with increasing ion number in peak.

Overtones: A final additional space charge effect was observed, unique to multi-reflection analyzers. It is possible, particularly when ion drift is poorly focused, for a small proportion of ions to strike the detector at the wrong number of oscillations. These additional false-positive peaks may be called overtones and arise at characteristic single oscillation time offsets (see Supplementary Figure 5). If space charge expands the energy spread of the ion cloud in the direction of ion drift down the elongate mirrors, it can push some proportion of ions beyond the system's energy acceptance, which will broaden the ion packet and may generate overtones at high ion number. Figure 10 shows this occurrence for an accumulation time scan of isolated MRFA ions, whereby the +1 overtone started to appear significantly after 3000 ions in peak, and grew to 0.3% by 6000 ions. Another scan was made with the analyzer drift focusing slightly detuned from its apex, by shifting the second prism deflector by -5V. In this case the overtones emerged slightly more readily and grew much more rapidly.

This emphasizes the importance of good instrument tuning, to remove false-positive signals as well as maximise sensitivity. In truth there are many other such sources in ToF spectra, such as scattered ions, unwanted fragmentation, and sample background and contaminants, so a fraction of a percent offscourings from rare intense peaks is not hugely significant. However, these peaks are theoretically easy to detect, and could be subtracted in post-processing should they prove an issue.

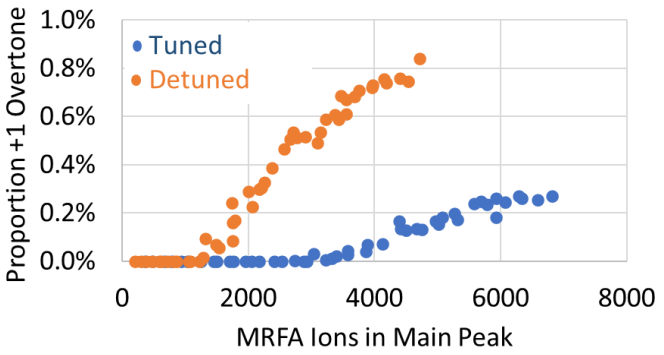

Figure 10. The appearance of MRFA peaks with incorrect numbers of oscillations (overtones) with increasing ion number and space charge.

Conclusion

Space charge effects were measured for the Astral mass analyzer incorporating converging ion trapping and ion focusing via converging ion mirrors. The influences of resonant effects, between similar m/z ions, become strong at ~10^3 ions in peak, but at high overall ion loads they are also somewhat mitigated by in-trap space charge. A single analyzer calibration was found to be suitable for a wide dynamic range of trapped ions, albeit with some compromise to the achievable resolution.

Whilst loss of resolving power was the most crucial space charge effect observed, it could be somewhat compensated for by adjustment of the focal plane position. Other issues emerged at higher charge numbers, including detectable coalescence of neighboring peaks, slight weakening of drift focal quality, and when the ion trap combined excessive loading with low trapping RF amplitude, an m/z shift of the poorly trapped high m/z ions.

It is expected that the interplay of in-trap and in-analyzer space charge effects, as well as the limiting circumstances described here, will help inform experiment design and the optimum usage of both the Astral analyzer and emergent ion trap and multi-reflection mass analyzers.

Acknowledgements

The authors would like to acknowledge the advice and support of colleagues throughout Thermo Fisher Scientific, upon whose shoulders this work has been built.

Declaration of Competing Interests

The authors declare the following competing financial interest(s): all authors are employees of Thermo Fisher Scientific, the manufacturer of instrumentation used in this research.

References

[1] Anderson, N. L., & Anderson, N. G. (2002). The human plasma proteome: history, character, and diagnostic prospects. *Molecular & cellular proteomics*, 1(11), 845-867.

[2] Liu, T., Qian, W. J., Gritsenko, M. A., Xiao, W., Moldawer, L. L., Kaushal, A., ... & Smith, R. D. (2006). High dynamic range characterization of the trauma patient plasma proteome. *Molecular & Cellular Proteomics*, 5(10), 1899-1913.

[3] Makarov, A., Denisov, E., Kholomeev, A., Balschun, W., Lange, O., Strupat, K., & Horning, S. (2006). Performance evaluation of a hybrid linear ion trap/orbitrap mass spectrometer. *Analytical chemistry*, 78(7), 2113-2120.

[4] Zhang, Z., Wu, S., Stenoien, D. L., & Paša-Tolić, L. (2014). High-throughput proteomics. *Annual review of analytical chemistry*, 7, 427-454.

[5] Eliuk, S., & Makarov, A. (2015). Evolution of Orbitrap mass spectrometry instrumentation. *Annu. Rev. Anal. Chem*, 8(1), 61-80.

[6] Michalski, A., Damoc, E., Lange, O., Denisov, E., Nolting, D., Müller, M., ... & Makarov, A. (2012). Ultra high resolution linear ion trap Orbitrap mass spectrometer (Orbitrap Elite) facilitates top down LC MS/MS and versatile peptide fragmentation modes. *Molecular & Cellular Proteomics*, 11(3)

[7] Grinfeld, D., Stewart, H., Skoblin, M., Denisov, E., Monastyrsky, M., & Makarov, A. (2019). Space-charge dynamics in Orbitrap mass spectrometers. *International Journal of Modern Physics A*, 34(36), 1942007.

[8] Mamyrin, B. A. (2001). Time-of-flight mass spectrometry (concepts, achievements, and prospects). *International Journal of Mass Spectrometry*, 206(3), 251-266.

[9] Mamyrin, B. A., Karataev, V. I., Shmikk, D. V., & Zagulin, V. A. (1973). The mass-reflectron, a new nonmagnetic time-of-flight mass spectrometer with high resolution. *Zh. Eksp. Teor. Fiz*, 64(1), 82-89.

[10] Wollnik, H., & Przewloka, M. (1990). Time-of-flight mass spectrometers with multiply reflected ion trajectories. International Journal of Mass Spectrometry and Ion Processes, 96(3), 267-274

[11] Wollnik, H., (1980) Time of flight mass spectrometer, German Patent DE3025764C2.

[12] Verentchikov, A. N., Yavor, M. I., Hasin, Y. I., & Gavrik, M. A. (2005). Multireflection planar time-of-flight mass analyzer. I: An analyzer for a parallel tandem spectrometer. *Technical Physics*, 50(1), 73-81

[13] Nazarenko L.M., Sekunova L.M., Yakushev E.M., (1989). "Time-of-flight mass spectrometer with multiple reflections" Soviet Patent No. SU1725289

[14] Kozlov B., Kirillov S. and Monahov A., Analysis of Coulomb interaction effects in high resolution TOF and electrostatic FT mass spectrometers in terms of phase space rotation, *Proceedings of the 60th ASMS Conference on Mass Spectrometry and Allied Topics*, Vancouver, Canada, 2012.

[15] Grinfeld, D., Giannakopulos, A. E., Kopaev, I., Makarov, A., Monastyrskiy, M., & Skoblin, M. (2014). Space-charge effects in an electrostatic multireflection ion trap. *European Journal of Mass Spectrometry*, *20*(2), 131-142

[16] Chernushevich, I. V., Loboda, A. V., & Thomson, B. A. (2001). An introduction to quadrupole–time-of-flight mass spectrometry. *Journal of mass spectrometry*, 36(8), 849-865

[17] Ibrahim, Y. M., Belov, M. E., Liyu, A. V., & Smith, R. D. (2008). Automated gain control ion funnel trap for orthogonal time-of-flight mass spectrometry. *Analytical chemistry*, 80(14), 5367-5376.

[18] Hardman, M., Makarov, A. A. (2003). Interfacing the Orbitrap mass analyzer to an electrospray source, *Analytical Chemistry*, 75, 1699-1705.

[19] Grinfeld, D. and Makarov, A. (2013). Multi-reflection mass spectrometer, United States Patent US9136102B2.

[20] Stewart, H., Grinfeld, D., Giannakopulos, A., Petzoldt, J., Shanley, T., Garland, M., ... & Hock, C. (2023). Parallelized Acquisition of Orbitrap and Astral Analyzers Enables High-Throughput Quantitative Analysis. *Analytical Chemistry*, 95(42), 15656-15664.

[21] Stewart, H., Grinfeld, D., Wagner, A., Kholomeev, A., Biel, M., Giannakopulos, A., ... & Hock, C. (2023). A Conjoined Rectilinear Collision Cell and Pulsed Extraction Ion Trap with Auxiliary DC Electrodes*. Journal of the American Society for Mass Spectrometry*. DOI: 10.1021/jasms.3c00311.

[22] Stewart, H., Grinfeld, D. and Wagner, A., (2022). Multi-reflection mass spectrometer, United Kingdom Patent Application GB2605395A.

[23] Rosenbusch, M., Wada, M., Chen, S., Takamine, A., Iimura, S., Hou, D., ... & Wollnik, H. (2021). The new MRTOF spectrograph for nuclear masses following RIBF's Zero Degree spectrometer, featuring new methodologies for ion selection and mirror optimization*. arXiv preprint arXiv:2110.11507*

[24] Wienholtz, F., Kreim, S., Rosenbusch, M., Schweikhard, L., & Wolf, R. N. (2017). Mass-selective ion ejection from multi-reflection time-of-flight devices via a pulsed in-trap lift. *International Journal of Mass Spectrometry*, 421, 285-293.

[25] Verentchikov, A. N., Yavor, M. I. and Pomozov, T. Y., Electrostatic ion mirrors, United States Patent US9396922B2.

[26] Kozlov, B., Galeev, G., Gavrik, M., Hasin, Y., … & Verentchikov, A. Space charge effects in multi-reflecting time-of-flight mass spectrometer. *Proceedings of the 54th ASMS Conference on Mass Spectrometry*, Seattle, WA, 2006.

[27] Grinfeld, D. E., Kopaev, I. A., Makarov, A. A., & Monastyrskiy, M. A. (2011). Equilibrium ion distribution modeling in rf ion traps and guides with regard to Coulomb effects. *Nuclear Instruments and Methods in Physics Research Section A: Accelerators, Spectrometers, Detectors and Associated Equipment*, 645(1), 141-145.

[28] Tolmachev, A. V., Udseth, H. R., & Smith, R. D. (2000). Radial stratification of ions as a function of mass to charge ratio in collisional cooling radio frequency multipoles used as ion guides or ion traps. *Rapid Communications in Mass Spectrometry*, 14(20), 1907-1913

[29] Verentchikov, A. N., Yavor, M. I., Hasin, Y. I., & Gavrik, M. A. (2005). Multireflection planar time-of-flight mass analyzer. II: The high-resolution mode. *Technical Physics*, 50(1), 82-86.